NUMERICAL ANALYSIS OF THREE-DIMENSIONAL STRUCTURE OF THE SEA BREEZE OVER SOUTHWESTERN BOHAI GULF

Wu Zengmao (吴增茂)

Institute of Physical Oceanography, Shandong College of Oceanology, Qingdao

Received December 16, 1986

ABSTRACT

In this paper, a simulation study is made on the sea breeze process over southwestern Bohai Gulf by use of the Pielke mesoscale meteorological model. The simulated results show that when a south wind of 8 m/s blows over the top of the model, a strong wind zone of 15—25 km wide with a maximum speed more than 14 m/s, which is close and nearly parallel to the south shore, will appear at 160 m above the sea surface. When a strong sea breeze penetrates inland, there often appears a thermal internal boundary layer (TIBL) near shore. The inversion above the TIBL can damp the vertical dispersion of atmospheric pollution. Besides, it is also found that, for a three-dimensional sea/land breeze circulation, if the divergence centre in the return flow departs vertically far from the correspondent convergence centre in the sea breeze, a centre of strong descending movement will be formed at the middle and upper levels of the return flow. The results in this paper is also applicable to the Laizhou Bay.

I. INTRODUCTION

We are often told by the personnel for the Bohai Offshore Oil Field weather prediction that it is very difficult to predict the sea surface wind at the Bohai Gulf, which may make trouble for the living supply to oil platforms and the operation of transport ships. Additionally, it is said that sometimes a vast sheet of low clouds suddenly appears along the coast line, which is a serious obstacle to the takeoff and landing of aircraft. As is known, the sea-land breeze is a very important mesoscale local circulation. It may cause the obvious diurnal variation in wind speed and direction as well as in vertical velocity in offshore and onshore areas of 100–200 km wide, and directly influence the development and movement of convective clouds there. Therefore, the sea-land breeze has an effect not only on the air pollution in coastal zones and offshore operation, but also on the flight training of air force near coast areas. For these reasons, it is of substantial importance to study the features and variations of sea breeze circulation.

In this paper, a numerical simulation is made on the three-dimensional structure of sea breeze over southwestern Bohai Gulf by use of the Pielke mesoscale model (Pielke, 1984; Mahrer and Pielke, 1977). The experiment was performed during the auther studied in the Swedish Meteorological and Hydrological Institute (SMHI). The simulation is not based on observed cases, owing to no enough time to get an available resolution map and meteorological data. The area studied looks like southwestern Bohai Gulf, and also like the same part of Laizhou Bay. Furthermore, the mean latitude of the area is taken as 37° N, which is a good approximation to the mean latitude for both areas. Therefore the results of the experiment are qualitatively reliable for either area. According to the shape of the coast line, the results of two experiments with northwesterly and southerly prevailing wind are analysed, in which the breeze process is assumed to happen in early May. Since land breeze is usually much weaker than sea breeze, only the latter process is discussed here.

II. NUMERICAL MODEL AND EXPERIMENT PROCEDURE

A detailed description of the model is omitted. In the following, only a summary of the model and the procedure of the experiments are presented. It is assumed in the model that the atmosphere is incompressible and in hydrostatic equilibrium. Moreover, the thermodynamic process of saturated air has not been taken into account. Cartesian coordinates are used with x direction westward, y southward and z vertically upward.

1. *Parameterization of Subgrid Scale Fluxes*

The model includes two parts in the vertical. The lower part is the surface layer of atmosphere which is parameterized with the similarity formulas (Businger, 1973), and above the surface layer is the upper part in which the exchange coefficients are evaluated in daytime and nighttime respectively with O'Brien (1970) and Blackadar (1979) formulas. The description of the former formula is omitted here, for it has been commonly used. The latter can be expressed as

$$K_m=K_\theta=\begin{cases} 1.1\,(R_{ic}-R_i)\,l^2\left|\dfrac{\partial V}{\partial z}\right|\Big/R_{ic}, & R_i\leqslant R_{ic} \\ 0, & R_i>R_{ic} \end{cases}$$

where K_m and K_θ are turbulence exchange coefficients for momentum and heat respectively; V is the horizontal wind vector; R_{ic} is the critical Richardson number, taken as 0.25; l is the mixing length and given by

$$l=\begin{cases} K_z & z<200m\,(K=0.35) \\ 70m & z\geqslant 200m \end{cases}.$$

2. *Boundary Conditions*

The domain simulated is 160×140 km with $\Delta x=\Delta y=5$ km. The top of the model is taken to be 7 km. In the vertical direction, except for the surface, the atmosphere is divided into 16 levels by an increasing interval with height. In the simulation topography is not taken into account, and the top of the model is set to keep constant. The land surface temperature is computed by a Newton-Raphson iteration solution to the heat balance equation for the surface. The sea surface temperature is taken as 13 °C. The mixing ratio of moisture keeps 8.4 g/kg at the sea surface and 4.0 g/kg at the land surface. It is assumed that there is no effect of mesoscale disturbance at the top, and no slip of fluid at $z=z_0$, here z_0 is the roughness parameter.

The lateral boundary conditions are zero gradient for all prognostic variables. Meanwhile gradually enlarged grids are employed for the four outermost circles to avoid the contamination of solution caused by lateral boundary effects.

3. *Numerical Integration and Initial Conditions*

In the model the locally one-dimensional integration scheme is employed. Advection terms are solved by the upstream interpolation on cubic splines, vertical diffusion terms by the further weighted Crank-Nicholson difference scheme, and horizontal diffusion terms are treated by highly selective filters—the implicit filters enhanced near the lateral boundaries with a view to eliminating shortwave noise.

The integration starts at sunrise ($t=0$, i. e. 0527 LT, 1 May) and it is assumed that at $t=0$, the atmosphere is barotropical and the fields of wind, temperature and humidity are horizontally homogeneous. The initial wind profile is obtained with a one-dimensional dynamic model. The author has found that the wind profile calculated by the original version has an obviously unreasonable bend, and after modification the simulated results get improved.

In order to study the effect of synoptic scale wind on sea-land breeze, the following experiments are made: (a) the wind at the upper boundary is 8 m/s northwesterly and, (b) 8 m/s southerly. It is assumed that the initial fields of temperature and humidity are identical for both experiments, and they are prescribed based on the observational data in Qingdao. A two-hour steady integration without consideration of surface heating is required to make the model get in equilibrium before simulation. During the period of the integration, the humidity field at lower levels is rapidly adjusted to meet the sea and land surface boundary conditions. Since the initial values of humidity is less important, so that only the initial values of wind and temperature are listed in Table 1.

Table 1. The Initial Values of Wind Component U, V (m/s) and Potential Temperature (K)

		Altitude z(m)															
		2	10	20	40	80	160	300	600	1000	1500	2100	2800	3700	4700	5700	7000
Test 1	U	−2.9	−4.1	−4.6	−5.1	−5.7	−6.3	−7.2	−5.7	−5.7	−5.7	−5.7	−5.7	−5.7	−5.7	−5.7	−5.7
	V	1.3	1.9	2.1	2.4	2.6	2.9	3.6	5.7	5.7	5.7	5.7	5.7	5.7	5.7	5.7	5.7
Test 2	U	1.4	2.0	2.2	2.5	2.7	2.9	2.9	0.0	0.0	0.0	0.0	0.0	0.0	0.0	0.0	0.0
	V	−3.1	−4.4	−4.9	−5.5	−6.1	−6.7	−8.0	−8.0	−8.0	−8.0	−8.0	−8.0	−8.0	−8.0	−8.0	−8.0
Potential Tem. (K)		286.0	286.0	286.0	286.1	286.3	286.6	287.2	288.3	289.6	291.2	292.8	295.0	297.7	300.8	303.9	308.0

III. RESULTS OF NUMERICAL SIMULATION

It is pointed out that in the following figures the plane coordinates are the same as in Fig. 1, so that the coordinates in the horizontal section diagrams to be discussed below are omitted. However, when a vertical cross section diagram is discussed, for the sake of clearness, not only are the horizontal and vertical coordinates marked, but also the site of the cross section in the model is given with IX or IY. Besides, the coastline is indicated with an arrow beneath the diagram. The wind barb in a horizontal wind diagram has the same meaning as in the weather map.

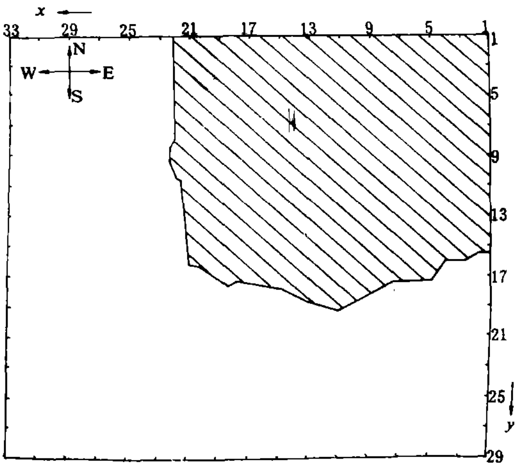

Fig. 1. The simulated domain with hatched area representing sea. The grid spacings for both x and y are taken to be 5 km, except for the four outermost circles.

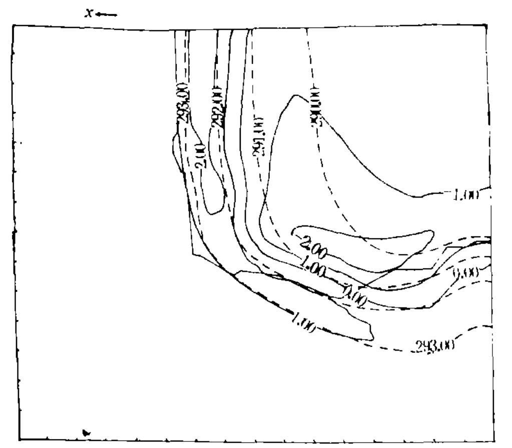

Fig. 2. Vertical velocity (solid lines, cm/s) and potential temperature (dashed lines, K) fields, at $z = 160$ m, after 4 hours of simulation.

1. *Results of Test* 1

In this experiment the wind is 8 m/s northwesterly at the upper boundary of the model. After the steady integration, the wind at the sea surface turns anticlockwise about 25° relative to the wind at the land surface since the sea surface is smoother than land. The results show that after 4 hours of simulation the sea breeze starts, which is consistent with the results given by Sun et al. (1979) and Wang et al. (personal communication) based on routine synoptic data. It can be seen from Fig. 2 that on the southern shore, due to a cool advection, there is a weak convergence zone inland; on the western shore with warm advection, there is a strong convergence zone offshore. This kind of feature is in line with the facts observed by Frank et al. (1967).

Additionally, we can find that the whole bow-shaped convergence zone extends upward to 1.5 km or higher and has a inland slope against the land surface (figure omitted). In the horizontal diagram, at the height of 1.5 km, the central zone of convergence above the southern shore penetrates deep into 20 km or more inland. Meanwhile, the central zone above the western shore also moves over land. It is not difficult to understand the fact that the convergence zone inclines toward low pressure from lower to higher levels.

A comparison of Fig.3a with 3b shows that at the 6th hour after sunrise, an area of strong divergence is formed over sea, and the central axis of the area inclines northwestward with increasing altitude, for the breeze related to the south coast is weaker and has a smaller vertical scale than that related to the west coast. In addition, it is worth noticing that, owing to the breeze front close to the west coast and a shallow TIBL (thermal internal boundary layer) thus formed (Ogawa et al., 1986), there is a sharp vertical shear of wind direction over the west coast, with a direction variation of about 90 degrees within a thickness of 100 m.

The results of the 8th hour (figure omitted) exhibit that the sea breeze gets much stronger and the convergence zone moves 10—15 km inland. A cool advection caused by

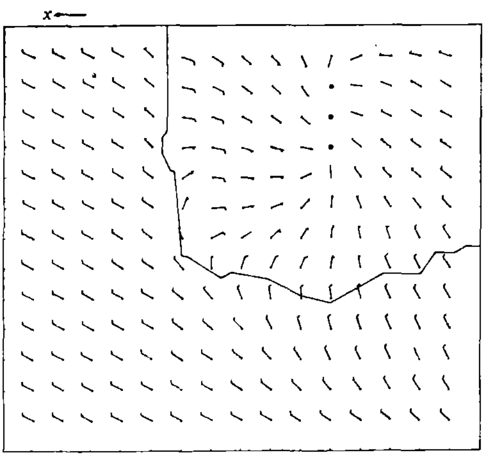

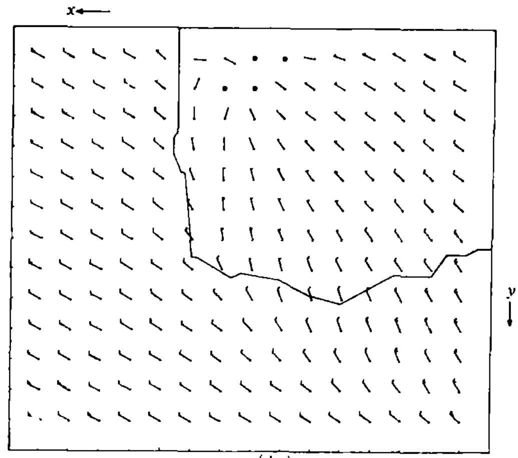

Fig. 3. Wind fields after 6 hours of simulation.
(a) $z=20$ m, and (b) $z=160$ m.

onshore synoptic wind reduces the sea breeze and convergence, however, the onshore wind can accelerate the inland advance rate of the breeze front. This fact was confirmed by Frank et al. (1967). Besides, since the breeze related to the west coast develops quickly and moves slowly, the divergence centre at the sea surface advances about 60 km toward ENE direction during 2 hours. It is evident that the movement is not controlled by the synoptic wind.

Figs. 4 and 5 respectively show the characteristics of the breeze structure in the vertical sections of east-west and north-south during the maximum surface temperature. Especially in Fig. 4a some interesting features are presented. If definding the breeze front by a wind-shift line and analysing Fig. 4a and 4b comprehensively, we can see from Fig. 4b that the alternating level between the sea breeze and its return flow is at about 800 m, which is substantially coincident with the observed results by Sun et al. (1979). As shown in Fig. 4a, the vertical velocity centre A is located at a height of about 1000 m over the surface front, and there appear two weak descending areas B_1 and B_2 to compensate ascending air. This characteristic structure is similar to the usual two-dimensional sea breeze.

It is known that in the circulation of a 2-D sea breeze, since the divergence centre in the return flow is located exactly over the convergence centre of sea breeze, the centre of vertical velocity appears at about the top level of the sea breeze, and the ascending velocity above the top level reduces rapidly with increasing altitude. Besides, there appears a weak compensate descending area at each side of the centre of ascending flow (see Figs. 4 and 5 in the paper by Wu, 1987).

Fig. 4a and 4b, however, show something very interesting. A descending centre C of 20 cm/s appears at the upper right side of A, about 1500 m high above it, In fact, it is a descending belt nearly parallel to the coast, as shown in Fig. 6. At the same time, two ascending centres D_1 and D_2 appear as well. A comparative analysis of Fig. 4a and 4b shows that a convergence area overlies on the centre A, and a divergence area occurs in the downstream. Consequently, the ascending area extends upward and the descending centre C appears in the middle and upper levels of the return flow. The interesting feature of structure can be attributed to the three-dimensional interaction between the southern and western branches of the sea breeze, respectively, including their components parallel to coast lines. Obviously, it is also related to the shape of the coast line and prevailing wind.

Although the results of this test are in accord with some observations, the above phenomenon still needs to further study and verify, since the detailed study and observation on three-dimensional structure of vertical velocity field of sea breeze are very seldom so far.

The ascending centre D_1 is closely related to the descending centre C, but it should be noticed that the results on the four outermost circles close to the lateral boundaries are not reliable. In the discussion of other figures, the availability of the results near the lateral boundaries should also be considered.

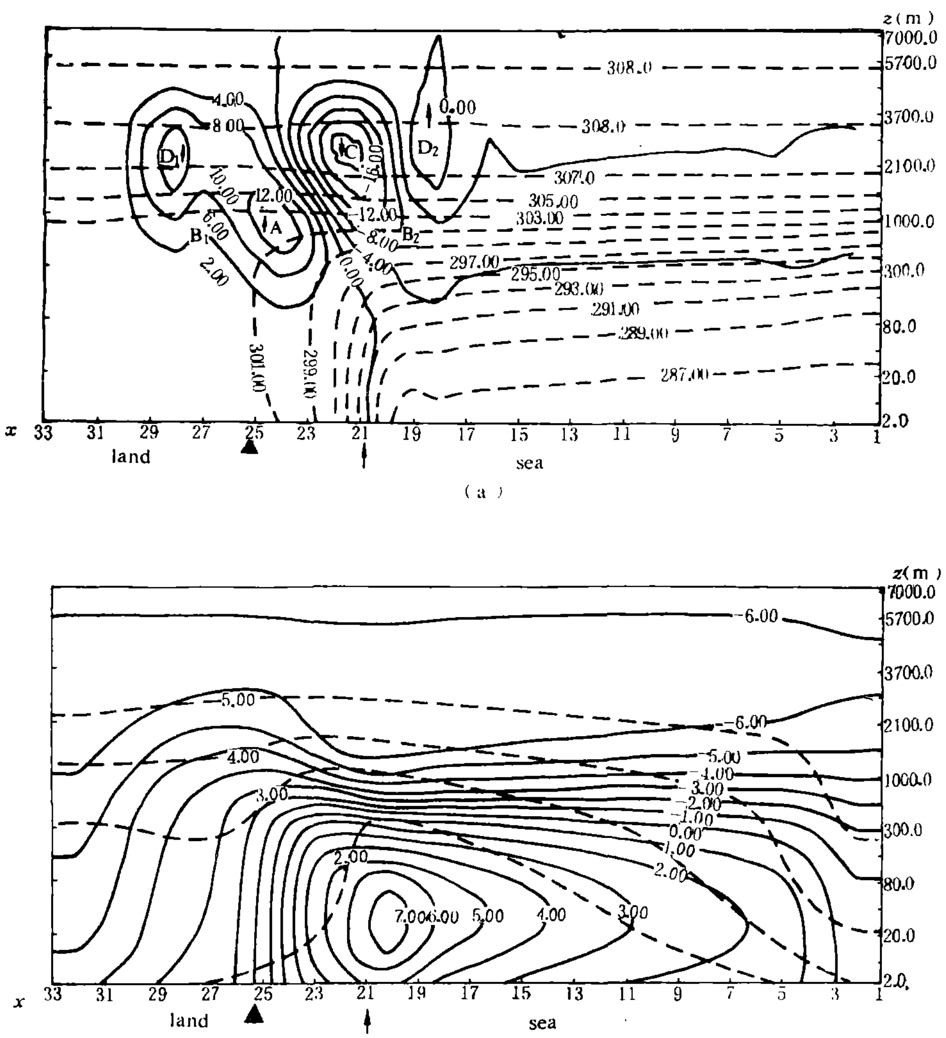

Fig. 4. At the 8th hour after sunrise in x-z section ($IY=14$), (a) vertical velocity (solid lines, cm/s) and potential temperature (dashed lines, K); (b) wind U component (solid lines, m/s) and V component (dashed lines, m/s). ▲ denotes the site of the breeze front.

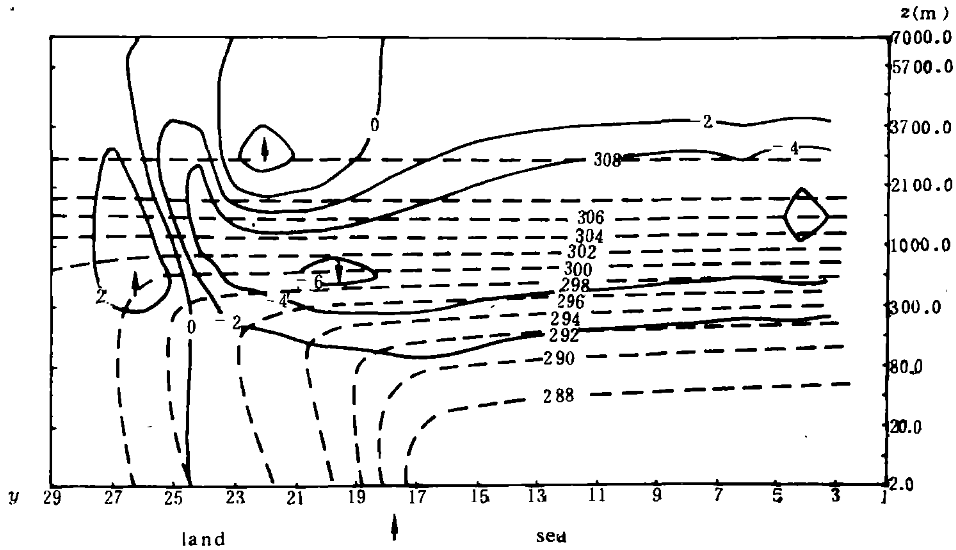

Fig. 5. Vertical velocity (solid lines, cm/s) and potential temperature (dashed lines, K) at the 8th hour after sunrise in y-z section ($IX=15$).

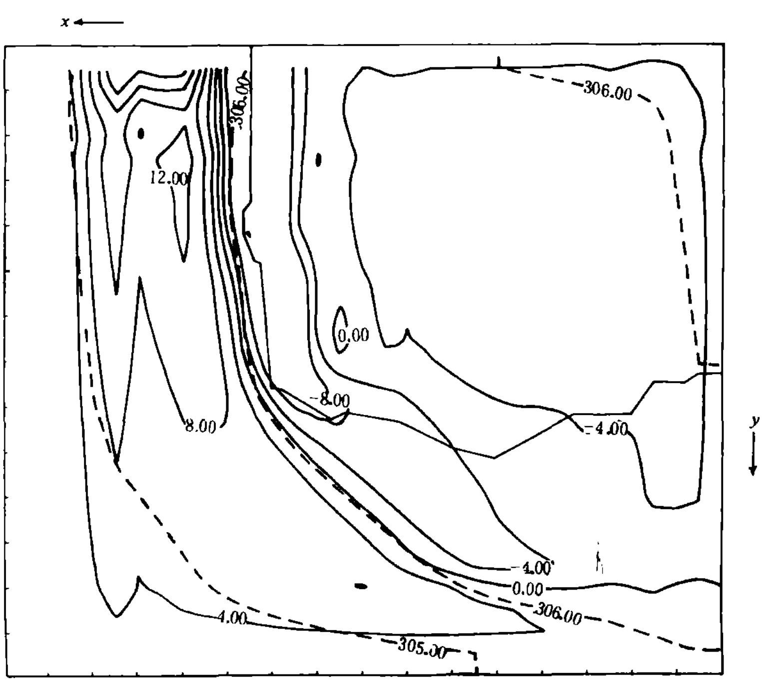

Fig. 6. As in Fig. 5, but for horizontal section at $z=1500$ m.

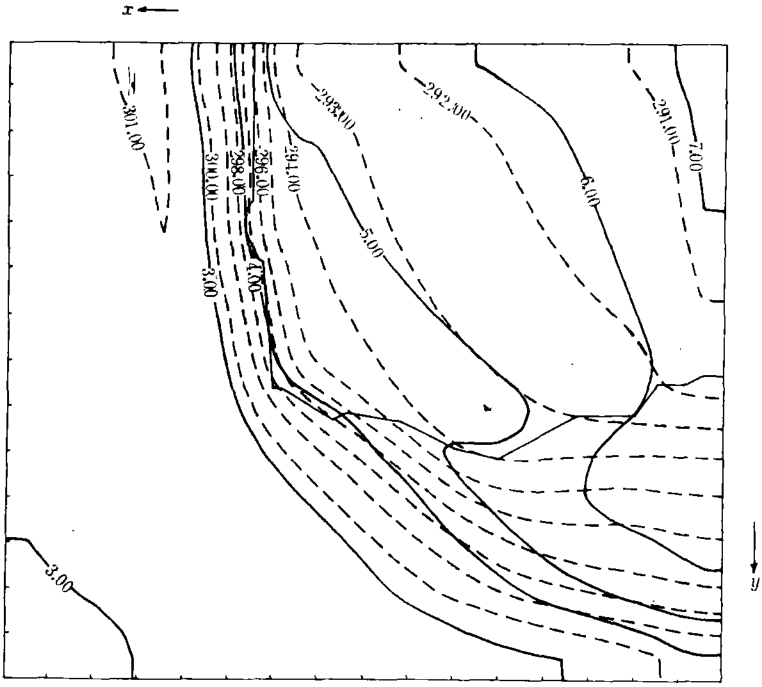

Fig. 7. Mixing ratio (solid lines, g/kg) and potential temperature (dashed lines, K) fields at the 8th hour after sunrise in horizontal section at $z=160$ m.

Comparing Fig. 5 with 4a, we can find a distinct difference between both vertical velocity fields respectively corresponding to west and south coasts. If the humidity field in Fig. 7 and the vertical velocity field in Fig. 6 are simultaneously analysed, we can find that under the control of the northwesterly prevailing wind each sea breeze front related to either the west or south coast corresponds a dry area. It follows that, in this case, convective clouds and rain are generally difficult to form due to insufficient moisture.

2. *Results of Test* 2

In this experiment wind is 8 m/s southerly at the top of the model. After steady integration, the wind direction at land surface is SSE, at sea surface ESE. Under the control of the background wind, the features of the sea breeze corresponding to the west coast are similar to those corresponding to the south coast in Test 1. However some interesting characteristics are presented by the breeze branch corresponding to the south coast. As shown in Fig. 8, by the 6th hour after sunrise a strong convergence zone is formed at sea surface near the south coast, meanwhile a weaker convergence zone which is formed at the west coast penetrates inland about 30 km. It may be inferred from the different positions of both convergence zones that, convergence forms along the west coast earlier than along the south coast. This phenomenon can be explained as follows: The cold advective air from sea surface may make the front air get into more unstable; on the contrary, the warm advective air from land, which usually overlies on the cold air at sea surface, may induce the air at sea surface to become more stable. Thus, in the former case the convective movement is easily produced, in the latter case, however, the adequate baroclinic energy has to be built up to overcome gravity and to form convection. This kind of phenomenon was observed by Frank et al. (1967) with a digitized rader.

It can be seen from Fig. 9 that at the 8th hour after sunrise a strong wind area occurs at 20 m above sea surface near the south coast, in which the maximum wind speed is 12

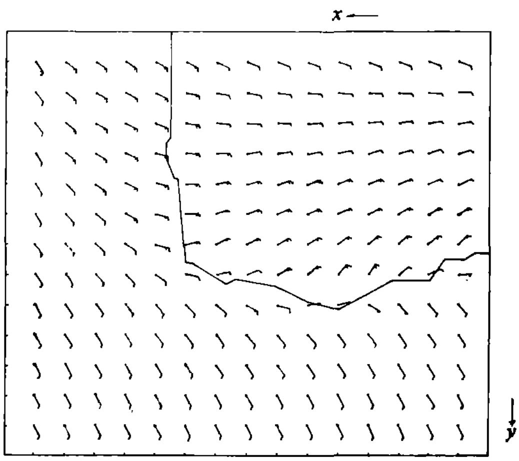

Fig. 8. Wind field at $z=20$ m level, at the 6th hour after sunrise.

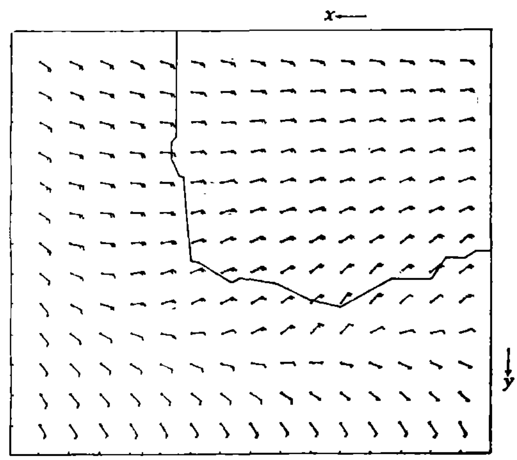

Fig. 9. Wind field at $z=20$ m level, at the 8th hour after sunrise.

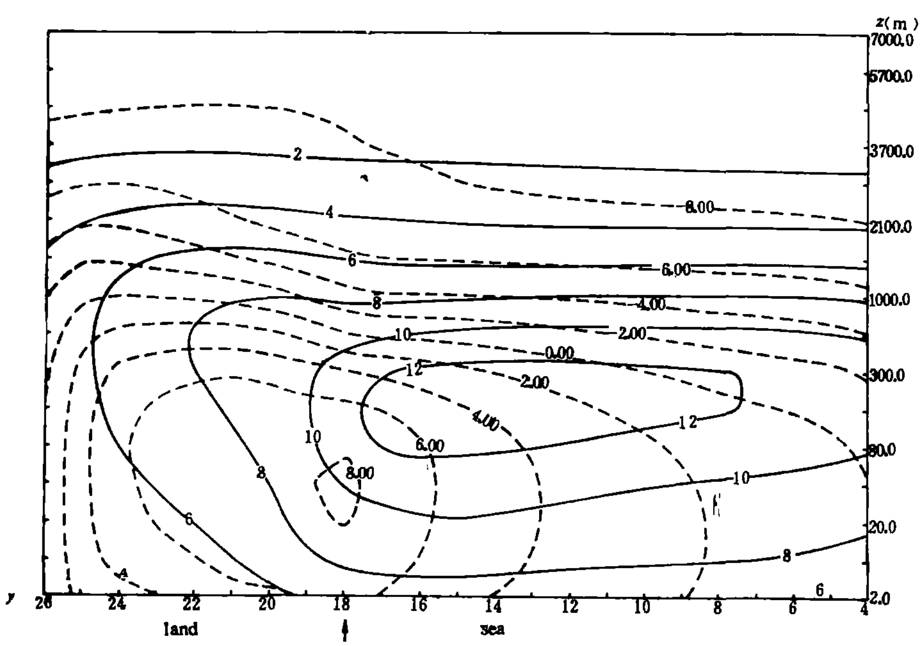

Fig. 10. Wind component U (solid lines, m/s) and V (dashed lines, m/s) in the y-z section ($IX=13$), at the 10th hour after sunrise.

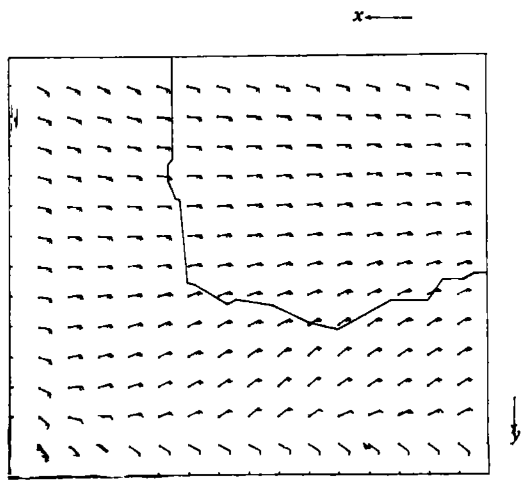

Fig. 11. Horizontal wind field at $z=160$ m level, at the 10th hour after sunrise.

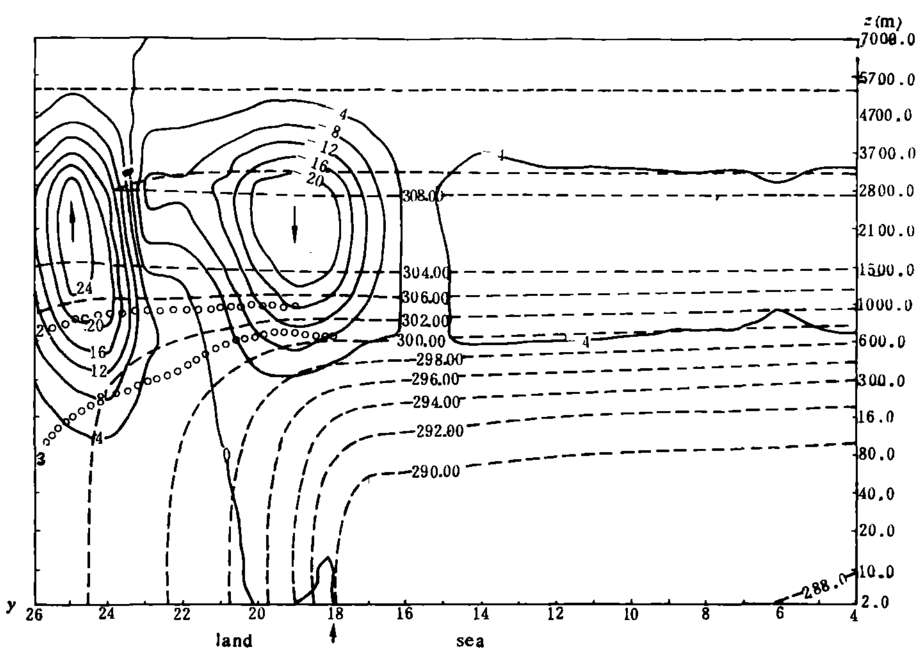

Fig. 12. As Fig. 10, but for the vertical velocity (solid lines, cm/s), potential temperature (dashed lines, K) and mixing ratio (circles, g/kg) fields.

m/s or more. Furthermore, the sea breeze continues to increase, 2 hours later it gets in the fully developed stage. The area with wind stronger than 12 m/s obviously enlarges, and still remains over the sea surface near the south coast (figure omitted). At the same time, the wind direction gradually veers clockwise.

The statistical results by Wang et al. (to be published) demonstrate that May has the maximum probability for the strong sea breeze occurrence at the south coast of the Bohai

Sea. Test 2 may be considered as one example of these results. Fig. 10 shows that, at the mature stage of the sea breeze circulation, a strong wind zone with maximum velocity more than 14 m/s appears at $z=160$ m level above the coast line. Fig. 11 shows the wind field at the level where the maximum wind core lies and the configuration of a strong wind zone, 15—20 km wide above sea surface and nearly parallel to the coast.

It can be seen from Fig. 12 that when sea breeze penetrates inland, a TIBL is formed; and above it appears a weak inversion, which prevents the air pollution from vertically transporting. Additionally, in comparison with results of Test 1, Fig. 12 shows that in Test 2 the moisture is relatively rich and ascending motion is energitic around the front of the south coast breeze, thereby it is easy to form convective clouds.

IV. CONCLUDING REMARKS

In this paper the three-dimensional structure characteristics of the sea breeze and their diurnal variations are discussed. In comparison with some statistic analyses and observations, we can see that simulated results are convincing. Although there are just two tests analysed, for the simulated coast line has a shape of a right angle, they represent four typical examples of sea breeze: (a) synoptic wind flows offshore at 45° angle; (b) onshore at 45 ° angle; (c) wind flows offshore and is normal to the coast line; and (d) parallel to the coast line.

It is assumed that, in the two tests all the conditions are same except the prevailing wind direction. From the analysis and comparison of simulated results, we come to the following conclusions:

(1) When synoptic wind is offshore and normal to the shoreline as (c), a strong sea/land circulation can be formed, and there appears a strong wind zone over sea near the coast. In this case the relatively moist air meets strong ascending motion very well and deep convective clouds are easily formed. In terms of the convective velocity over the sea breeze fronts, the above four cases should be arranged as: (c) strong, (a) less strong, (d) weak, and (b) weakest.

(2) The inland advance rate of breeze front is determined by both the averaged large-scale wind at lower levels and the front moving velocity relative to the air ahead, which has been discussed in detail by Mathews (1982). Furthermore, Wu (1987) physically analysed the velocity of the front. It may be concluded that the stronger the sea breeze is, the slower its front moves in relation to the air ahead. According to the inland advance rate of the front, the four cases are arranged as (b) fast, (d) less fast, (a)slow, and (c) slowest. This estimation has been confirmed by some observations.

(3) There are many factors affecting sea breeze. Assuming that the background wind is not too strong and there is no synoptic scale disturbance, and neglecting the change of other factors, we can say that the stronger the offshore synoptic wind is, the stronger the sea breeze circulation is, and the slower the breeze progresses inland. Conversely, the stronger the onshore synoptic wind is, the weaker the sea breeze is, but the faster the sea breeze progresses inland.

Although the results obtained are convincing, the further observational and theoretical verifications on the conclusions are still needed. It is particularly worth studying and examining in depth that in the upper and middle parts of the return flow appears a strong descending centre, which represents the reaction between both sea breeze branches respectively corresponding to the south and west coasts.

The author would like to thank Dr. S. Bodin who showed a great interest and support in this work, and also to thank Drs. P. Kallberg and K. Haggkvist for many constructive discussions and comments, especially for heartily guiding him in work with ECMWF computer. A special thank is devoted to Prof. R. A. Pielke (Colorado State University) for permitting him to work with their model.

REFERENCES

Atkinson, B. W. (1981), *Mesoscale Atmospheric Circulations*, Academic Press, London.

Frank, N. L. et al. (1967), Summer shower distribution over the Florida Peninsula as deduced from digitized radar data, *J. Appl. Met.*, **6**: 309—316.

Mahrer, Y. and Pielke, R. A. (1977), A numerical study of the airflow over irregular terrain, *Beitrage Zur Physik der Atmosphere*, **50**: 98—113.

Mathews, J. H. (1982), The sea breeze——forecasting aspects, *Aust. Met. Mag.*, **30**: 205—209.

Ogawa, Y. et al. (1986), Observation of lake freeze penetration and subsequent development of the thermal internal boundary layer for the Nanticoke II. Shoreline diffusion experiment, *Bound. Layer Met.*, **35**: 207—230.

Pielke, R. A. (1974), A three-dimensional numerical model of the sea breeze over south Florida., *Mon. Wea. Rev.*, **102**: 115—139.

Pielke, R. A. (1984), *Mesoscale Meteorological Modeling*, Academic Press, London.

Sun kuoying, et al. (1979), The sea breeze in the coastal region of Jinxi County, Collected Papers on Geophysics (Atmo. Physics), Peking University, 31—44 (in Chinese).

Wu Zengmao (1987), Numerical study of lake-land breeze over lake Vattern Sweden., *Advances in Atmospheric Sciences*, **4**: 198—209.